Internal character dictates transition dynamics between isolation and cohesive grouping

Pedro D. Manrique,[1] Pak Ming Hui,[2] and Neil F. Johnson[1]
[1]*Department of Physics, University of Miami, Coral Gables, Florida 33126, USA*
[2]*Department of Physics, Chinese University of Hong Kong, Shatin, Hong Kong, China*
(Received 20 June 2015; revised manuscript received 18 October 2015; published 2 December 2015)

We show that accounting for internal character among interacting heterogeneous entities generates rich transition behavior between isolation and cohesive dynamical grouping. Our analytical and numerical calculations reveal different critical points arising for different character-dependent grouping mechanisms. These critical points move in opposite directions as the population's diversity decreases. Our analytical theory may help explain why a particular class of universality is so common in the real world, despite the fundamental differences in the underlying entities. It also correctly predicts the nonmonotonic temporal variation in connectivity observed recently in one such system.

DOI: 10.1103/PhysRevE.92.062803 PACS number(s): 89.65.Gh, 87.23.Ge, 87.23.Kg

I. INTRODUCTION

Dynamical grouping underlies a myriad of collective phenomena across the physical, biological, chemical, economic, and social sciences [1–8]. Whether the underlying N objects are particles, people, or proteins, the issue of whether they evolve as isolated individuals or aggregates has significant consequences at the macrolevel [7–13]. Superradiance is driven by two-level systems coupling coherently via a background boson mode [14]; many neurodegenerative diseases are driven by aggregation of proteins [15]; large market movements are driven by traders' herding [16–18]; insurgencies are driven by informal human groupings [19–22] as are gangs and online guilds [23]; brain activity features collective neuronal avalanches [24]; and many-body coherence phenomena are impacted by connectivity within exotic materials [25,26] and networks [11,12].

It is tempting to try applying physics models of interacting, identical particles to describe grouping dynamics in living systems. However, a serious shortcoming is that the underlying objects (e.g., people, cells, and animals) are typically not identical and it is this heterogeneity that typically dictates their interactions and ultimately their collective behavior. Even simple cells of a given type can have chemical, physical, and conformational differences that affect their interactions, while for humans it is usually the characteristics of other group members that dictate whether individuals join or leave [27,28]. Outstanding questions are therefore how this diversity in individual characters affects the dynamics of groups [27–31] and how this individual-level heterogeneity can be reconciled with the emergent universality observed across many diverse real-world phenomena.

This paper attempts to address these questions by adding a simple, continuous character variable x_i to each object i and then allowing objects' characters to influence how they interact with each other. We assign static x_i's randomly from a given distribution $q(x)$, though this should be generalized in future work, e.g., to incorporate experience. A single scalar parameter has already been adopted in other contexts within the social science literature [29]. Breaking a link in systems such as insurgencies [19,20,32], financial trading [16,17], neuronal systems [24], and quantum systems [25] (e.g., through a loss of common purpose, loss of trust, loss of coordination, or loss of coherence, respectively) can lead to complete fragmentation of the group (cluster) [16–20,33]. We therefore implement a character-driven fission-fusion mechanism (Fig. 1) that mimics these features, producing sparse networks that are visually similar to those observed empirically [Fig. 1(b)]. Previous work [30,31,34,35] including in the absence of character suggests that our main conclusions could hold for a variety of model generalizations.

II. MODEL

We define the similarity between objects i and j as $S_{ij} \equiv 1 - |x_i - x_j|$. Though we choose $0 \leqslant \{x_i\} \leqslant 1$, wider ranges do not affect our main conclusions. Objects i and j with similar characters have S_{ij} near unity while those with dissimilar characters have S_{ij} near zero. At each time step t, with probability p an as-yet nonexistent link is randomly chosen as a candidate to form. If it forms following the grouping rules based on S_{ij} (see below and Table I) it will join together the two groups to which i and j belong [Fig. 1(a)]. With probability $1 - p$, an existing link is randomly chosen as a candidate to fragment. If it fragments following the grouping rules, the group within which it resides also fragments, mimicking the loss of common purpose, loss of trust, loss of coordination, or loss of coherence mentioned above [Fig. 1(a)].

We first consider each simulation being run using one (and only one) of the following grouping mechanisms. For M1, groups favor similar characters (i.e., favors kinship) as in Fig. 1(c). At a link-forming time step, the probability that the candidate link actually forms is S_{ij}. At a link-breaking time step, the probability that the candidate link actually breaks is $1 - S_{ij}$. For M2, groups favor diverse characters (i.e., arguably more like a team) as in Fig. 1(d). At a link-forming time step, the probability that the candidate link actually forms is $1 - S_{ij}$. At a link-breaking time step, the probability that the candidate link actually breaks is S_{ij}. For comparison, we also consider intermediate (M3) and character-free (M4) grouping mechanisms. Grouping mechanisms M4 does not use character as a rule for group formation. See Table I.

A. Numerical results

Figure 2 shows that even for a uniform character distribution $q(x)$, rich behavior emerges. As p increases, the average

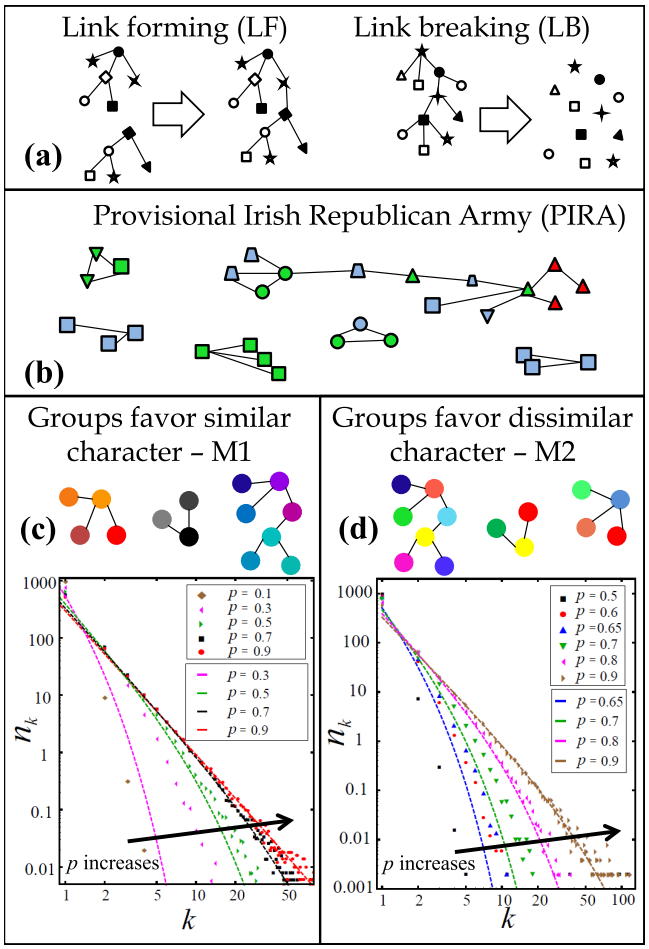

FIG. 1. (Color online) (a) Our model of interacting characters comprises two types of process: link formation leading to joining two groups and link breaking leading to group fragmentation. (b) Representative portion of PIRA insurgency network in Northern Ireland, adapted from Ref. [32]. Different symbols and colors represent different character types (e.g., bomb maker). It is slightly more connected than our model since all empirical link information is aggregated over a year [32]. (c) Groups favoring similar characters (i.e., like kinship) illustrated by similar shades. Underneath, group size distribution n_k showing simulation (symbols) and analytical (lines) results for different p values. (d) Same as (c) but now for groups favoring diverse characters (i.e., like a team).

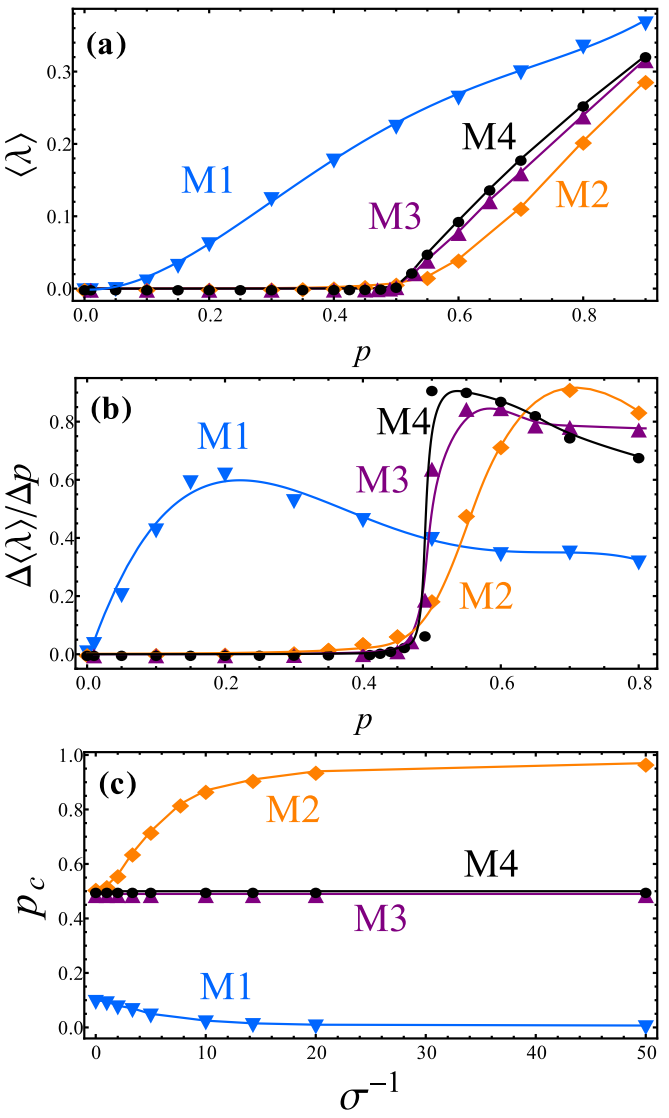

FIG. 2. (Color online) (a) Plot of $\langle\lambda\rangle$ versus p for $N = 10^4$ objects. Grouping mechanism M1 (blue inverted triangles) favors similar characters, e.g., kinship; M2 (orange diamonds) favors diverse characters, i.e., teamlike; M3 (triangles) is intermediate between M1 and M2; and M4 (black circles) is character-free. (b) Rate of change. Data points are calculated numerically for a uniform distribution of character values $q(x)$, while the lines are a best fit through these data points. (c) Plot of p_c for M1–M4 versus inverse standard deviation σ^{-1} for a Gaussian character distribution $q(x)$ centered on $\mu = 0.5$.

number of links per object $\langle\lambda\rangle$ increases from zero, indicating groups spontaneously forming from a population of isolates. Figure 2(b) shows the corresponding rate of change. The position and shape of the onsets depend on the group mechanism, with the M2 onset more abrupt than M1 but requiring much higher p. This implies that high-diversity groups and teams need to be encouraged by externally establishing a high p ($> p_c$), while kinship groups will naturally arise for almost

TABLE I. Values associated with different grouping mechanisms.

Grouping mechanism	Link-forming probability	Link-breaking probability	p_c (mean-field theory)	p_c (numerical simulation)	F	Q
M1 (e.g., kinship)	S_{ij}	$1 - S_{ij}$	3/11	0.10	2/3	1/4
M2 (e.g., team)	$1 - S_{ij}$	S_{ij}	3/5	0.51	1/3	1/2
M3 intermediate	S_{ij}	S_{ij}	9/17	0.49	2/3	3/4
M4 character-free	1	1	1/2	0.50	1	1

any p. Interestingly, the M1 and M2 onsets are less sharp than the intermediate M3 or the character-free M4. This suggests that real-world populations in which character dictates the grouping dynamics will show far more glassy transitions indicative of frustrated dynamics as compared to the sharp ones in character-free physics models. Results shown are averages over simulations with $N = 10^4$ objects, with each simulation comprising 10^5 time steps and data collected in the steady state. (See later Fig. 5 for other N values.)

B. Analytical approach

Our analytical analysis is a mean-field approach, starting with the coupled differential equations for n_k, the number of groups of size k at time step t for $k \leqslant N$:

$$\dot{n}_k = -(1-p)Q\frac{(k-1)n_k}{\sum_{r=2}^{\infty}(r-1)n_r} - 2Fp\frac{kn_k}{N^2}\sum_{r=1}^{\infty} rn_r + \frac{Fp}{N^2}\sum_{r=1}^{k} rn_r(k-r)n_{k-r}, \quad k \geqslant 2 \tag{1}$$

$$\dot{n}_1 = (1-p)Q\frac{\sum_{k=2}^{\infty}k(k-1)n_k}{\sum_{r=2}^{\infty}(r-1)n_r} - 2pF\frac{n_1}{N^2}\sum_{r=1}^{\infty} rn_r, \tag{2}$$

where F is a mean-field probability of a link being formed between two randomly chosen objects, while Q is a mean-field probability that an arbitrarily chosen link will break and hence that group will fragment. Since our focus is on networks that are naturally sparse [19,20], we take a group of size k as having $k-1$ links [19,20] in Eq. (1), though any number $O(k)$ would generate similar conclusions. In the steady state, these equations yield two possible solutions for the number of isolated individuals (see the Appendix): $n_1 = N$ or $n_1 = \frac{pF+(1-p)Q}{2pF}N$. Since $n_1 \leqslant N$, a transition will arise when $[pF + (1-p)Q] = 2pF$ from a population comprising 100% isolates to one with cohesive groups, i.e., at the critical point

$$p_c = Q(F+Q)^{-1}. \tag{3}$$

For $p > p_c$, each n_k for $k \geqslant 2$ changes from zero to the exact expression

$$n_k = \left|\frac{1}{2}!\left[2k\gamma(k!)\left(\frac{1}{2}-k\right)!\right]^{-1}(4\gamma n_1)^k\right| \tag{4}$$

where

$$\gamma = pF(N-n_1)\{N[Q(1-p)N + 2pF(N-n_1)]\}^{-1}. \tag{5}$$

We can evaluate F and Q analytically to obtain p_c for grouping mechanisms M1–M4: For a uniform character distribution $q(x)$, the probability density function (PDF) $f(y)$ of the similarity $y = S_{ij}$ is given by $f(y) = 2y$, with $y \in [0,1]$. For mechanism M1, the probability F that two objects will be linked is $\int_0^1 f(y)y\,dy = 2/3$. Similarly, the PDF of y associated with links is $g(y) = 3y^2$, hence the probability Q that a randomly selected link breaks is $\int_0^1 g(y)(1-y)dy = 1/4$. For M2, $g(y) = 6(1-y)y$. This procedure yields the theoretical values in Table I.

Figures 1(c) and 1(d) and Table I show good agreement between numerical simulation and our mean-field theory for $\{n_k\}$ and $\{p_c\}$. Differences are due to neglect of higher-order correlations. Equation (4) further reduces (see the Appendix) to the approximate form for $p > p_c$:

$$n_k = \frac{N}{2\sqrt{\pi}}\frac{p(1-p_c)}{p-p_c}\left[1-\left(\frac{p_c(1-p)}{p(1-p_c)}\right)^2\right]^k k^{-5/2}. \tag{6}$$

Equation (6) predicts an approximately exponential cutoff at high k that depends on the grouping mechanism through $p_c = Q(F+Q)^{-1}$, together with a 5/2 power-law exponent that does not. As data from real-world systems improves, it should be possible to estimate p_c and p, and hence Q/F, to infer likely character-driven grouping mechanisms in a given system.

Figure 2(c) shows that p_c shifts in opposite directions for M1 and M2 as the heterogeneity of the underlying population is reduced, using a Gaussian character distribution $q(x)$ with mean $\mu = 0.5$ and standard deviation σ. To the extent that M1 and M2 represent simplified versions of kinship and teamlike grouping dynamics, respectively, this observation suggests that teams require an ever higher p to form as a population becomes more homogeneous, with the population eventually comprising completely isolated individuals for all p. By contrast, kin groups require an ever lower p to form. Figure 3 shows the regime diagram. It bounds the parameter's region where our model yields to the creation of groups or where objects are isolated. The group cohesion regime is

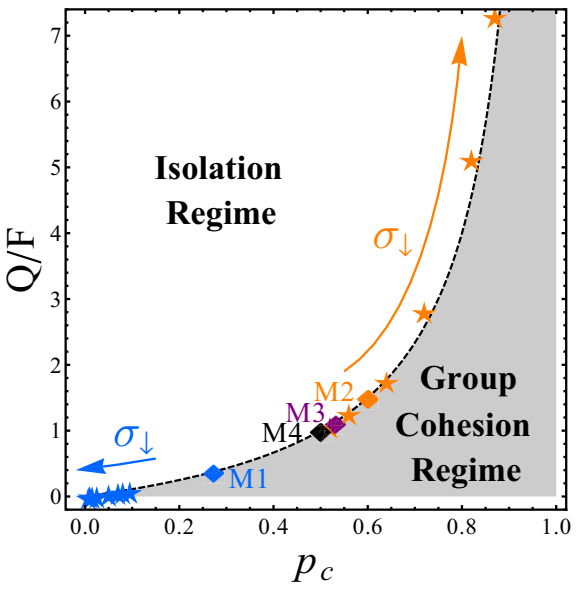

FIG. 3. (Color online) Regime diagram illustrating the parameter range corresponding to isolation and group cohesion. The curved regime boundary is our mean-field analytical result $p \equiv p_c = Q(F+Q)^{-1}$. Diamonds show p_c in the case of uniform character distribution $q(x)$ for M1–M4. Stars show numerical results for p_c with Gaussian $q(x)$ from Fig. 2(c). For M1, blue stars show that p_c moves toward the lower left part of the curve with decreasing standard deviation σ. For M2, orange stars show that p_c moves toward the upper right part of the curve with decreasing standard deviation σ. Hence the critical points p_c for M1 and M2 move in opposite directions as the diversity σ is reduced.

characterized by a common macroscopic order; the group's size distribution n_k. Regardless of the formation mechanism, n_k follows a 2.5 power-law distribution as illustrated in Figs. 1(c) and 1(d) and predicted by our mean-field approach in Eq. (6). Therefore, our model goes from a disordered regime of isolated objects to an ordered one of group formation whose sizes share a common macroscopic structure. In addition, the numerical simulation results lie remarkably close to the analytic curve $Q/F = p_c(1-p_c)^{-1}$, providing further support for our mean-field analysis.

III. REAL-WORLD COMPARISONS

While we are not suggesting that our simple model is an accurate representation of any particular real-world system, it is interesting to note that the $5/2$ exponent is exactly that observed empirically for (i) the severity of attacks inflicted by insurgent groups on a civilian population, indicating the size distribution of the insurgent groups [21,22]; (ii) the distribution of stock transaction sizes, indicating the herd sizes of similar-minded traders [17]; (iii) the size distribution of neuronal avalanches, given avalanche initiation by a randomly chosen neuron (i.e., $kk^{-5/2} \equiv k^{-3/2}$ [24]); and (iv) the size distribution of pockets of superconducting coherence in fragmented materials [25]. It is also very close to the values of 2.3 obtained from a study of 100 gangs in Chicago and separately in Manchoukuo [36]. Future detailed empirical work is required to clarify the underlying mechanisms of these diverse systems to understand the extent to which they might be consistent with the mechanisms considered here. However, these empirical observations will hopefully serve to motivate further interest in our model.

We can however make a simple but nonetheless instructive comparison to the real-world Provisional Irish Republican Army (PIRA) system [Fig. 1(b)], which is the best-known insurgency network to date [32]. Although the data are still unfortunately insufficient to infer the actual grouping mechanism since links are aggregated over years, which is why it appears more dense than snapshots of our model, we can test our model against the empirical finding that the PIRA underwent a bottom-up transition over time: from a rather homogeneous organization toward teamlike structures facilitated through a process of individual contact. We start our model PIRA population with an M1 grouping mechanism favoring similar character links. An individual is introduced who uses an M2 grouping mechanism favoring diverse character links and hence favoring team formation and who is able to spread its use to anyone with whom he or she instantaneously shares a cluster. They then become spreaders (susceptible → infected), reflecting the fact that the teamlike structure became recognized as improving the PIRA's operational efficacy and hence got reinforced over time by contacts at grass-roots level. Figure 4 shows the resulting prediction concerning connectivity from our model and the actual PIRA data. For both cases, we measure the average number of links per actor (object) λ and the fraction of isolated actors n_1/N. We note that Fig. 4 has multiple dynamical features that are not necessarily dependent and yet our model is still able to capture their overall nonlinear dependence. By contrast, we find that other group formation mechanisms do not reproduce these features.

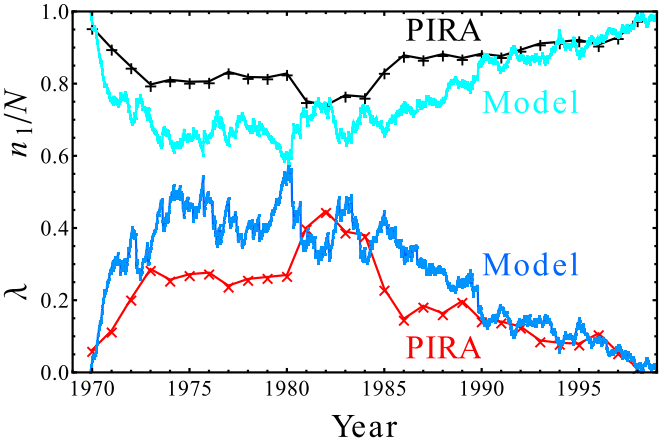

FIG. 4. (Color online) Our model's prediction (line without crosses) vs actual PIRA temporal variation (line with crosses) for the fraction of isolated individuals n_1/N (top two curves) and the ratio between the total number of links in the network and the total number of individuals λ (bottom two curves). The PIRA data are from Ref. [32]. The model considers equally formation and fragmentation time steps ($p = 0.5$). At $t = 0$, most of the objects follow M1 rules with only one object following M2 rules. However, this object spreads M2 rules as it join other groups. Over time, this spreading serves to drive the formation rules from mostly M1 to M2, just like the bottom-up transition from homogeneous to teamlike structure experienced by the PIRA. A time step in the model corresponds to a day in terms of the real data.

IV. SYSTEM SIZE AND COMPOSITION

Figure 5 illustrates how similar transition results emerge for a given mechanism, as N increases. Specifically, Fig. 5 shows

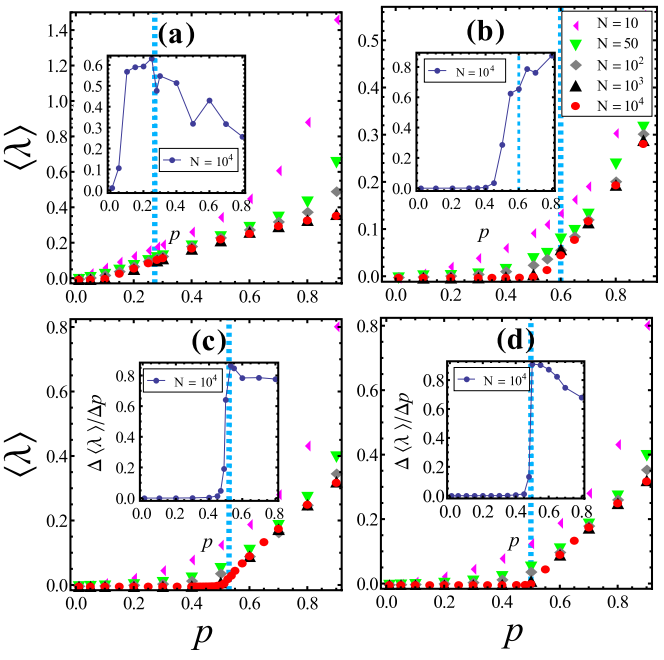

FIG. 5. (Color online) Results for $\langle\lambda\rangle$ as a function of p for different values of N for (a) M1, (b) M2, (c) M3, and (d) M4. Vertical dashed lines show the critical point p_c predicted by our mean-field theory. Insets show the rate of change.

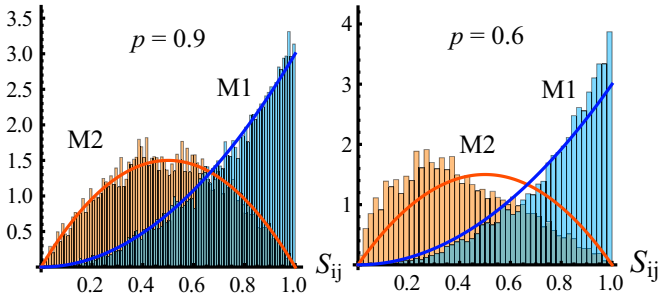

FIG. 6. (Color online) Distribution of similarities $S_{ij} \equiv 1 - |x_i - x_j|$ within groups for M1 and M2, from simulation with different values of the parameter p for a uniform character distribution. The histogram is a snapshot of the numerical simulation in the steady state for 10^4 objects. Solid lines are the corresponding mean-field results: $g(y) = 3y^2$ for M1 and $g(y) = 6(1-y)y$ for M2, where $y = S_{ij}$.

$\langle\lambda\rangle$ as a function of p for the grouping mechanisms M1–M4 and different values of the number of objects N. For M2–M4, the transition gets sharper in the region of the critical point p_c as N is increases, as predicted by the mean-field approach (dashed vertical line). Insets show the rate of change for $N = 10^4$. Interestingly for M1, the transition remains smooth and hence more glassy in appearance than the others. In terms of the distribution of links within the groups for the different mechanisms, Fig. 6 illustrates this for M1 and M2 in the case of a uniform character distribution. It shows their nontrivial nature based on their respective tendencies to favor similarity and dissimilarity, respectively. Solid lines are the PDF $g(y)$ associated with link formation from our mean-field approach. The agreement is noteworthy, especially for larger p. Future work should attempt to predict these distributions for model variants beyond those in Table I.

V. SUMMARY

In summary, we have shown that rich transition dynamics emerge when the objects in a population possess an internal character variable. Our analytical theory offers an explanation for why a particular statistical universality is so ubiquitous in real-world systems, despite fundamental differences in the composite objects and their interactions. Our findings also help open a path toward understanding how different grouping mechanisms (e.g., M1 vs M2) affect spreading in realistic (i.e., heterogeneous) populations. In physical systems, the different group mechanisms (e.g., M1 vs M2) may conceivably be used to mimic the tuning of particle-particle interactions in an exotic material, with p acting like an inverse temperature.

ACKNOWLEDGMENTS

We are grateful to Chaoming Song and Stefan Wuchty for discussions and John Horgan and Paul Gill for sharing their PIRA data and specialist knowledge.

APPENDIX: ANALYTIC DERIVATION OF n_k

The two master equations are as follows: For $k \geqslant 2$,

$$\frac{\partial n_k}{\partial t} = -P\,(\text{size } k \text{ group fragments}) + P\,(\text{smaller groups combine to size } k) - P\,(\text{size } k \text{ groups joins other groups}), \tag{A1}$$

and for $k = 1$,

$$\frac{\partial n_1}{\partial t} = -P\,(\text{single actor joins other group}) + P\,(\text{big group fragments}). \tag{A2}$$

Mathematically, the equation for $k \geqslant 2$ becomes

$$\frac{\partial n_k}{\partial t} = -(1-p)Q\frac{(k-1)n_k}{\sum_{r=2}^{\infty}(r-1)n_r} - 2pF\frac{kn_k}{N^2}\sum_{r=1}^{\infty} rn_r + pF\frac{1}{N^2}\sum_{r=1}^{k} rn_r(k-r)n_{k-r}. \tag{A3}$$

Here n_k is the number of groups of size k. The equation for $k = 1$ becomes

$$\frac{\partial n_1}{\partial t} = -2pF\frac{n_1}{N^2}\sum_{r=1}^{\infty} rn_r + (1-p)Q\frac{\sum_{k=2}^{\infty} k(k-1)n_k}{\sum_{r=2}^{\infty}(r-1)n_r}. \tag{A4}$$

In the steady state, the left-hand side of each of these equations becomes zero. Using $\sum_{r=1}^{\infty} rn_r = N$ and $(k-1)n_k \approx kn_k$, we get from Eq. (A3) that

$$kn_k = \frac{pF(N-n_1)}{N[Q(1-p)N + 2pF(N-n_1)]}\sum_{r=1}^{k} rn_r(k-r)n_{k-r} \equiv \gamma\sum_{r=1}^{k} rn_r(k-r)n_{k-r}. \tag{A5}$$

Let $g(w) = \sum_{r=2}^{\infty} rn_r e^{-wr}$, hence

$$\begin{aligned} g(w)^2 &= (2n_2e^{-2w} + 3n_3e^{-3w} + 4n_4e^{-4w} + \cdots)(2n_2e^{-2w} + 3n_3e^{-3w} + 4n_4e^{-4w} + \cdots) \\ &= (3n_1n_3 + 4n_2^2 + 3n_1n_3)e^{-4w} + (4n_1n_4 + 6n_2n_3 + 6n_2n_3 + 4n_1n_4)e^{-5w} + \cdots - 6n_1n_3e^{-4w} - 8n_1n_4e^{-5w} - \cdots \\ &= \sum_{r=1}^{4} rn_r(4-r)n_{4-r}e^{-4w} + \sum_{r=1}^{5} rn_r(5-r)n_{5-r}e^{-5w} + \cdots - 6n_1n_3e^{-4w} - 8n_1n_4e^{-5w} - \cdots \\ &= \frac{1}{\gamma}[2n_2e^{-2w} + 3n_3e^{-3w} + 4n_4e^{-4w} + 5n_4e^{-5w} + \cdots - 2n_2e^{-2w} - 3n_3e^{-3w}] \end{aligned}$$

$$-2n_1e^{-w}(2n_2e^{-2w}+3n_3e^{-3w}+4n_4e^{-4w}+\cdots-2n_2e^{-2w})$$
$$=\frac{1}{\gamma}[g(w)-2n_2e^{-2w}-3n_3e^{-3w}]-2n_1e^{-w}[g(w)-2n_2e^{-2w}]. \quad \text{(A6)}$$

From Eq. (A5) we have $2n_2=\gamma n_1^2$ and $3n_3=4\gamma n_1 n_2$, so Eq. (A6) becomes

$$g(w)^2-\left[\frac{1}{\gamma}-2n_1e^{-w}\right]g(w)+n_1^2e^{-2w}=0. \quad \text{(A7)}$$

For $w=0$ we have $g(0)=\sum_{r=2}^{\infty}rn_r=N-n_1$, hence we get $g(0)=\gamma N^2$ and

$$n_1=N-g(0)=N(1-\gamma N). \quad \text{(A8)}$$

Note that γ is itself a function of n_1. Equation (A8) can be solved for n_1. The solutions are

$$n_1=N \text{ or } n_1=\frac{pF+(1-p)Q}{2pF}N. \quad \text{(A9)}$$

The smaller root is kept as the physical solution. Under the condition that $\frac{pF+(1-p)Q}{2pF}\geqslant 1$, i.e.,

$$p\leqslant\frac{Q}{F+Q}, \quad \text{(A10)}$$

n_1 becomes N, indicating that there are only isolated actors in the system, as claimed earlier.

Consider now the case of any general value of w. The quadratic equation (A7) can be solved to give

$$g(w)=\frac{1}{2\gamma}-n_1e^{-w}\pm\frac{1}{2\gamma}\sqrt{1-4\gamma n_1e^{-w}}. \quad \text{(A11)}$$

The solution with the negative sign in the square root is kept. Using the property that $\sqrt{1+x}=\sum_{k=0}^{\infty}\frac{(\frac{1}{2})!}{k!(\frac{1}{2}-k)!}x^k$, we have

$$g(w)=-\frac{1}{2\gamma}\sum_{k=2}^{\infty}\frac{(\frac{1}{2})!}{k!(\frac{1}{2}-k)!}(-4\gamma n_1e^{-w})^k$$
$$=\sum_{k=2}^{\infty}kn_ke^{-kw}. \quad \text{(A12)}$$

Therefore, the group size distribution for $k\geqslant 2$ is

$$n_k=-\frac{1}{2\gamma k}\frac{(\frac{1}{2})!}{k!(\frac{1}{2}-k)!}(-4\gamma n_1)^k. \quad \text{(A13)}$$

This is the full (exact) form of the group distribution $\{n_s\}$. Note that this expression also holds for n_1, i.e., plugging in $k=1$ gives the previous n_1.

Using the property of the gamma function,

$$\left(\frac{1}{2}-n\right)!=\Gamma\left(\frac{1}{2}-n+1\right)=\frac{(-1)^{n-1}2^{n-1}\sqrt{\pi}}{(2n-3)!!}. \quad \text{(A14)}$$

For $n=0$ we have $(\frac{1}{2})!=\frac{\sqrt{\pi}}{2}$. The $(2n-3)!!$ term can be expressed as

$$(2n-3)!!=\frac{(2n-2)!}{2^{n-1}(n-1)!}. \quad \text{(A15)}$$

Therefore,

$$\frac{1}{k}\frac{(\frac{1}{2})!}{k!(\frac{1}{2}-k)!}=\frac{2(2k-2)!}{(-1)^{k-1}(k!)^2 4^k}. \quad \text{(A16)}$$

Substituting into Eq. (A13) and using the Stirling approximation

$$\ln(z!)\approx\tfrac{1}{2}\ln 2\pi+\left(z+\tfrac{1}{2}\right)\ln z-z, \quad \text{(A17)}$$

we have for large k that $\ln n_k$ is given approximately by the expression

$$k\ln(\gamma n_1)+\left(2k-\tfrac{3}{2}\right)\ln(2k-2)-(2k-2)$$
$$-2\left(k+\tfrac{1}{2}\right)\ln k+2k-\tfrac{1}{2}\ln 2\pi-\ln\gamma. \quad \text{(A18)}$$

Taking $2k-2\approx 2k$, we have

$$\ln n_k\approx k\ln(\gamma n_1)+\left(2k-\tfrac{3}{2}\right)\ln(2k)-2k$$
$$-2\left(k+\tfrac{1}{2}\right)\ln k+2k-\tfrac{1}{2}\ln 2\pi-\ln\gamma$$
$$=k\ln(\gamma n_1)-\tfrac{5}{2}\ln k+2k\ln 2-\tfrac{3}{2}\ln 2-\tfrac{1}{2}\ln 2\pi-\ln\gamma$$
$$=k\ln(4\gamma n_1)-\tfrac{5}{2}\ln k-2\ln 2-\tfrac{1}{2}\ln\pi-\ln\gamma. \quad \text{(A19)}$$

Therefore,

$$n_k\sim\frac{1}{4\gamma\sqrt{\pi}}(4\gamma n_1)^k k^{-5/2}, \quad \text{(A20)}$$

which is equivalent to Eq. (6).

[1] M. Anghel, Z. Toroczkai, K. E. Bassler, and G. Korniss, Phys. Rev. Lett. **92**, 058701 (2004).

[2] A. Soulier and T. Halpin-Healy, Phys. Rev. Lett. **90**, 258103 (2003).

[3] B. Goncalves and N. Perra, *Social Phenomena: Data Analytics and Modeling* (Springer, Berlin, 2015).

[4] G. Palla, A. L. Barabasi, and T. Vicsek, Nature (London) **446**, 664 (2007).

[5] P. L. Krapivsky, S. Redner, and E. Ben-Naim, *A Kinetic View of Statistical Physics* (Cambridge University Press, Cambridge, 2010).

[6] E. Estrada, Phys. Rev. E **88**, 042811 (2013).

[7] C. Song, S. Havlin, and H. Makse, Nat. Phys. **2**, 275 (2006).

[8] G. Caldarelli, *Scale-Free Networks: Complex Webs in Nature and Technology* (Oxford University Press, Oxford, 2007).

[9] A. L. Barabasi and H. E. Stanley, *Fractal Concepts in Surface Growth* (Cambridge University Press, Cambridge, 1995).
[10] F. Radicchi and S. Fortunato, Phys. Rev. E **81**, 036110 (2010).
[11] J. Nagler, A. Levina, and M. Timme, Nat. Phys. **7**, 265 (2011).
[12] P. S. Dodds, D. J. Watts, and C. F. Sabel, Proc. Natl. Acad. Sci. U.S.A **100**, 12516 (2003).
[13] I. D. Couzin *et al.*, Nature (London) **433**, 513 (2005).
[14] O. L. Acevedo, L. Quiroga, F. J. Rodríguez, and N. F. Johnson, Phys. Rev. Lett. **112**, 030403 (2014).
[15] Z. Zhao *et al.*, J. Comput. Theor. Nanosci. **6**, 1 (2009).
[16] J. L. Egido, L. M. Robledo, and V. Martin, Phys. Rev. Lett. **85**, 26 (2000).
[17] X. Gabaix *et al.*, Q. J. Econ. **121**, 461 (2006).
[18] R. D'Hulst and G. J. Rodgers, Int. J. Theor. Appl. Fin. **03**, 609 (2000).
[19] J. Robb, *Brave New War* (Wiley, New York, 2007).
[20] D. Kilcullen, *The Accidental Guerrilla* (Oxford University Press, Oxford, 2009).
[21] J. C. Bohorquez *et al.*, Nature (London) **462**, 911 (2009).
[22] N. F. Johnson *et al.*, Sci. Rep. **3**, 3463 (2013).
[23] N. F. Johnson, C. Xu, Z. Zhao, N. Ducheneaut, N. Yee, G. Tita, and P. M. Hui, Phys. Rev. E **79**, 066117 (2009).
[24] D. R. Chialvo, Nat. Phys. **6**, 744 (2010).
[25] M. Fratini *et al.*, Nature (London) **466**, 841 (2010).
[26] N. F. Johnson *et al.*, AIP Adv. **1**, 012114 (2011).
[27] S. Wuchty, B. Jones, and B. Uzzi, Science **316**, 1036 (2007).
[28] D. R. Forsyth, *Group Dynamics* (Cengage, New York, 2013).
[29] D. Centola *et al.*, J. Confl. Resolut. **51**, 905 (2007).
[30] A. Wyld and G. J. Rodgers, Physica A **374**, 491 (2007).
[31] Z. Zhao, J. P. Calderon, C. Xu, G. Zhao, D. Fenn, D. Sornette, R. Crane, P. M. Hui, and N. F. Johnson, Phys. Rev. E **81**, 056107 (2010).
[32] V. Asal, P. Gill, R. K. Rethemeyer, and J. Horgan, Journal of Conflict Resolution **59**, 401 (2015).
[33] T. Caro, *Antipredator Defenses in Birds and Mammals* (University of Chicago Press, Chicago, 2005).
[34] B. Ruszczycki *et al.*, Eur. Phys. J. B **72**, 289 (2009).
[35] N. F. Johnson, P. Manrique, and P. M. Hui, J. Stat. Phys. **151**, 395 (2013).
[36] L. F. Richardson, *Statistics of Deadly Quarrels* (Boxwood, Pacific Grove, 1960).